Journal of Korean Association of Crystal Growth
Vol. 4, No. 2 (1994) 148-156

Directional solidification by the skull melting in the $YO_{1.5}$-BaO-CuO system

Yong S. Chung and D. Norman Hill
School of Materials Science and Eng., Georgia Inst. of Tech., Atlanta, GA 30332, USA

Skull melting 방법에 의한 $YO_{1.5}$-BaO-CuO계의 방향적 결정성장

정용선, D. Norman Hill
죠지아 주립공과대학교 재료공학과, 아틀란타, GA 30332, USA

Abstract Three compositions in the system of $YO_{1.5}$-BaO-CuO were grown using a cold crucible (skull) melting technique with a 50 kW R. F. induction generator operating at 4 MHz as the power source. The starting materials were prepared by conventional ceramic powder processing methods, loaded into the skull, and melted at about 1200℃. For this study, compositions near the $YBa_2Cu_3O_X$ region were selected. The growth rates used ranged from 4 cm/hr to 0.25 cm/hr. The relation between the microstructure and the starting composition of each ingot was determined using metallograph, X-ray diffraction, and energy dispersive X-ray analysis. Both $YBa_2Cu_3O_X$ and Y_2BaCuO_5 needle-shaped crystals, aligned with the growth direction, were formed in the CuO-$BaCuO_2$ eutectic matrix of the $YBa_2Cu_7O_X$ and $YBa_3Cu_{11}O_X$ ingot.

요 약 $YBa_2Cu_3O_X$상 부근의 3가지 조성을 skull melting 방법으로 4 MHz에서 녹인 후 방향적 결정성장을 시켰다. 일반적인 무기재료 공정방법으로 처리된 분말을 skull에 넣은 후 1200℃ 부근에서 용융시켰다. 사용한 성장속도는 4～0.25 cm/hr이었으며, 금속현미경, X-선 회절기, EDX 등을 이용해서 제조된 시편을 조사하여 사용한 분말의 조성에 따른 시편의 미세조직의 변화를 관찰하였다. $YBa_2Cu_7O_X$와 $YBa_3Cu_{11}O_X$ 시편의 대표적인 미세조직은 성장방향으로 자라난 침상형태의 $YBa_2Cu_3O_X$와 Y_2BaCuO_5 상이 CuO-$BaCuO_2$의 공융 조직상 사이에 생성된 것으로 나타났다.

1. Introduction

Since the discovery of a superconducting phase with a critical temperature (T_C) higher than 30 K in the La-Ba-Cu-O system by Bednorz and Muller [1], many scientists have investigated ceramic superconductors with similar compositions. In 1987, a superconducting phase having a T_C above 90 K, $YBa_2Cu_3O_X$ (hereafter referred to as YBCO), was reported by Wu *et al.* [2].

In order to utilize the YBCO phase, this material must be able to carry large currents at temperatures above 77 K (under high magnetic fields). Bulk YBCO superconductors, however, have displayed critical current density (J_C) values of 100 ~ 1000 A/cm^2, whereas J_C values of the Nb-Ti, Nb_3Sn and single-crystal YBCO superconductors are above 10^5 A/cm^2. According to Ekin [3], this phenomenon is due to the weak links between high-J_C grains;two possible causes of weak links have been suggested. The first possibility is the presence of non-high-T_C phases or impurities localized in the grain boundary regions [4]. In bulk materials, the relative density is usually 70 % and the grain to grain connection is relatively poor. The second possibility is two dimensional anisotropy of the YBCO superconducting phase [5,6]. When the grains are aligned with the high-J_C axes(a-b plane) in the direction of current, the critical current is often higher than that of bulk sintered sample, in which orientation of the crystal axes tends to be random.

Many scientists are trying to improve the properties of YBCO thin films using several different methods, including a melt growth technique. The main purpose of the melt growth method is to achieve the aligned microstructure of superconducting phases for increasing the critical current density [7, 8]. Generally the directional solidification is better way than any other methods to control the microstructures of the bulk materials. For example, S. Jin *et al.* [8] made the well-oriented YBCO specimen which was consisted of the long, plate-shape grains without pores. The value of J_C at zero-field was improved to 10^4 A/cm^2. They concluded that improvement of J_C value was due to (i) the preferred orientation of the superconducting phase, (ii) the reduction of porosity with the enhanced connectivity, and (iii) the cleaner and fewer grain boundaries. Therefore it is important to know second phases which can be precipitated between the YBCO phase in the specimen produced by the melt growth technique.

The one of problems in the directional growth technique is coming from the reaction of the molten YBCO material with the crucible during the long hours of operations, because the YBCO materials are very reactive with almost of the refractory or substrate materials near 900℃, where it is frequently processed [9-13]. The reaction or interdiffusion between the substrate and the superconducting material leads to the formation of undesirable second phases and degrades the superconductivity, usually resulting in a broadening of the superconducting transition. To eliminate the reaction with crucible, it is desirable to use a cold crucible (skull) melting technique. The skull melting method, using direct dissipation of electrical en-

ergy to heat materials, has several benefits with respect to conventional ceramic processing methods. The first is the elimination of the reaction with the crucible because no contact is required between the heat source and the materials. Second, heating can be restricted to a localized area. Third, high temperatures can be obtained rapidly.

Three compositions for the directional growth were chosen near the composition of the YBCO phase in order to study the change of the liquid composition and the phases precipitated during the non-equilibrium solidification in the Y-Ba-Cu-O system : i) YBCO composition, ii) CuO rich composition and iii) BaO-CuO rich composition, compared with the YBCO composition.

2. Experimental procedure

Yttrium oxide (99.99 % purity) was used as a yttrium source, while barium carbonate and cupric oxide powders (reagent grade) were used as sources of barium and copper, respectively. The starting powders were ball-milled in a high density polyethylene jar for three hours, using distilled water as a milling medium. After ball milling, the powder was dried, ground, and then screened through a U. S. standard No. 20 sieve to calcine the powder. The dried powder was loaded loosely in an alumina sagger and calcined in air, holding for 12 hours at T_{max} and for 3 hours at 400℃ during the cooling (Table 1). The calcined powder was ground and screened in the same manner as the dried powder.

The R. F. generator (50 kW) used for skull melting was operated at 4 MHz. The skull was made of copper for high thermal conductivity and was 5 cm in diameter. The outer copper tubes that comprised the skull were 9 mm in diameter and 30.3 cm long, the inner tube was 6 mm in diameter and 28 cm long. A two-turn water-cooled working coil was used in all the experiments. The growth rate was determined by lowering the skull through the coupling zone.

The calcined powders were loaded on the skull as shown in Fig. 1. The powder in the bottom area of the skull was compacted by a vibrator to better seal the spaces between the copper tubes and contain the melt; in order to avoid the reduction of the oxide powder, the

Table 1
Experimental conditions of the directional growth by the skull melting

Composition name	Compositon (m/o)	Calcine temperature (T_{max}, ℃)	Growth rate (cm/hr)
$YBa_2Cu_3O_X$	$17Y^1+33B^2+50C^3$	850	2.0
$YBa_2Cu_7O_X$	10Y+20B+70C	890	4.0
$YBa_5Cu_{11}O_X$	6Y+30B+64C	850	0.25

[1] $Y = \frac{1}{2}Y_2O_3$, [2] $B = BaCO_3$, [3] $C = CuO$

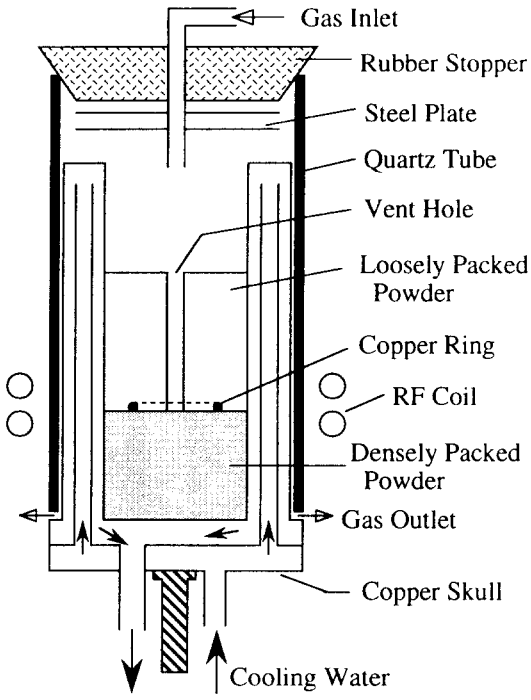

Fig. 1. Powder loading geometry for the skull melting.

copper wire ring (3.17 g), instead of graphite disc, was placed on the top of the compacted powder as a starter. The powder in the upper section was filled loosely, without any vibration or compaction, leaving a hole in the center to release gas pressure as the powder melted. Two stainless steel heat shields were used to protect the rubber seal. A quartz tube, three inches in diameter, was placed just outside the skull to maintain the oxygen over-pressure atmosphere.

After the initial powder charge had melted at about 1200℃, the calcined powder was added to the skull continuously in small amounts. When the total amount of powder consumed reached about 2 kg, powder addition was halted and the rubber stopper was inserted in the quartz tube. The temperature of the melt was kept below 1000℃ approximately. Oxygen gas flowed over the melt at a rate of 400 cc/min and the skull was lowered through the coil at a fixed rate. Micro-optical pyrometer was used to measure the temperature of the melt inside the skull during solidifications. The other processing parameters are summarized with the compositions in Table 1; the locations of the starting composition are shown on the phase diagram (Fig. 2) [14].

The ingots produced were about 10 cm long. The top half was cut into transverse sections and longitudinal sections. For metallographic analysis, each section was mounted and polished using 1 and 3 μm alumina powder. Kerosene was used as a grinding and polishing medium, with acetone serving to clean the samples. Sometimes it was necessary to anneal the sectioned samples in an oxygen atmosphere because of incomplete oxidation during the

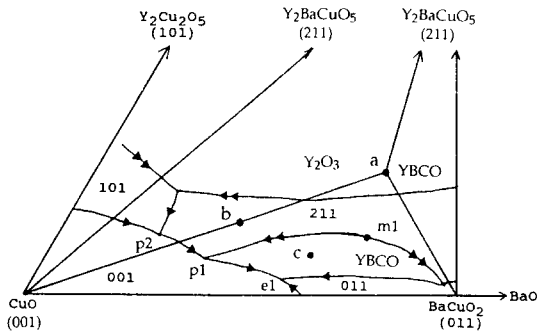

Fig. 2. Phase diagram indicating the starting composition for the skull melting; (a) $YBa_2Cu_3O_X$, (b) $YBa_2Cu_7O_X$ and (c) $YBa_5Cu_{11}O_X$, from Aselage [14]. (The double arrows depict a peritectic reaction.)

solidification due to low oxygen diffusion rate into the melt. The annealing temperature was dependent on the sample composition. The samples were heated at a rate of 560℃/hour, held for 12 hours, and cooled at the furnace cooling rate. The annealed samples were mounted and ground in the same manner as the unannealed samples.

The microstructures of the sectioned samples were examined using a metallographic microscope and an SEM, with an EDX for chemical analysis. Phase analysis was accomplished by X-ray diffractometer (XRD).

3. Results and discussion

3.1. $YBa_2Cu_3O_X$ composition

The microstructure of the annealed sample is shown in Fig. 3. As is evident in the micrographs, there were no pores nor needle-shaped crystals, as were observed in other samples. The dark and light grey areas corresponded to the Y_2BaCuO_5 (211) and YBCO phases, respectively. The dark grey phase (211) was usually surrounded by the envelope of the light grey phase (YBCO), showing the typical microstructure formed by the peritectic transformation [15]. According to the morphology of the YBCO grains in this specimen (Fig. 3(b)), the peritectic reaction was occurred by the solute diffusion through the solid[16]. The white phase was determined to be copper oxide by EDX analysis. The black areas in the matrix appear to be barium cuprate, not pores. The phases which were confirmed by XRD, were YBCO, $BaCuO_2$ (011), 211, copper oxide, and yttrium oxide.

Under the equilibrium state during the solidification, the Y_2O_3 (100) primary phase would precipitate in the liquid. When the liquid composition reached the boundary of the 211 and 100 phase, the 211 phase would begin to crystallize and the 100 phase would disappear by the peritetic reaction with the liquid. The 211 primary phase would be formed in the liq-

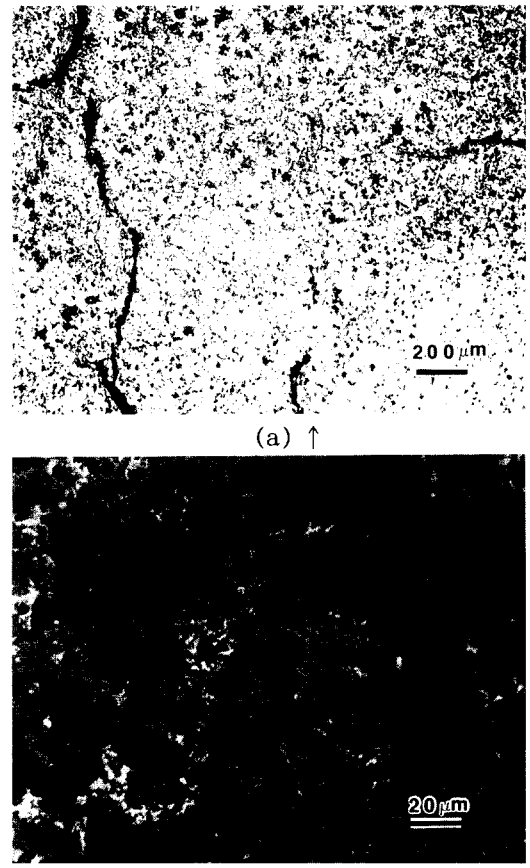

Fig. 3. Microstructures of the annealed $YBa_2Cu_3O_X$ ingot; (a) longitudinal section (50×) and (b) transverse section (500×). (↑ : growth direction).

uid when the composition of the liquid was between those of the YBCO and m1 (see Fig. 2). The 211 primary phase would precipitate until the liquid composition reached the boundary of the 211 and YBCO phases, and then all the 211 phase would be transformed to YBCO by the peritectic reaction. The crystallization path would stop at point m1. However, as shown in the Fig. 3, the solidified ingot did not reach this equilibrium state. The 100 and 211 phases were not transformed completely, and the liquid composition changed, moving toward the CuO and BaO-rich region. Therefore the microstructure included both CuO and $BaCuO_2$-CuO eutectic phases between the YBCO grains.

3.2. $YBa_2Cu_7O_X$ composition

The typical microstructures of the longitudinal and transverse sections of the ingot are shown in Fig. 4. As shown in the Fig. 4 (a), the needle-shaped grains crystallized with a good alignment along the growth direction. In the unannealed samples it was difficult to see the microstructure clearly (due to hydration) except for the needle-shaped phase. When annealed at 695℃, a very fine eutectic structure could be seen (Fig. 5). This eutectic structure was proved to be CuO-$BaCuO_2$. The white neeled-shaped grains (W) were CuO and the grey needle-shaped grains (G) were datermined to be 211 and YBCO. Micrographs of the YBCO phase and the eutectic structure in the unannealed $YBa_2Cu_7O_X$ sample were taken using SEM (Fig. 6). The discontinuous phase and the matrix in Fig. 6 (b) were CuO and $BaCuO_2$, respectively. CuO appeared as a major phase with 011, 211, YBCO and unknown phases in the X-ray diffraction pattern.

According to the phase diagram, the 211 primary phase will begin to form in the liquid and the YBCO phase will precipitate along the boundary curve between the YBCO and the 211, as the 211 phase is expended. At point p1, all the 211 phase will disappear and the CuO (001) phase will crystallize. The crystallization

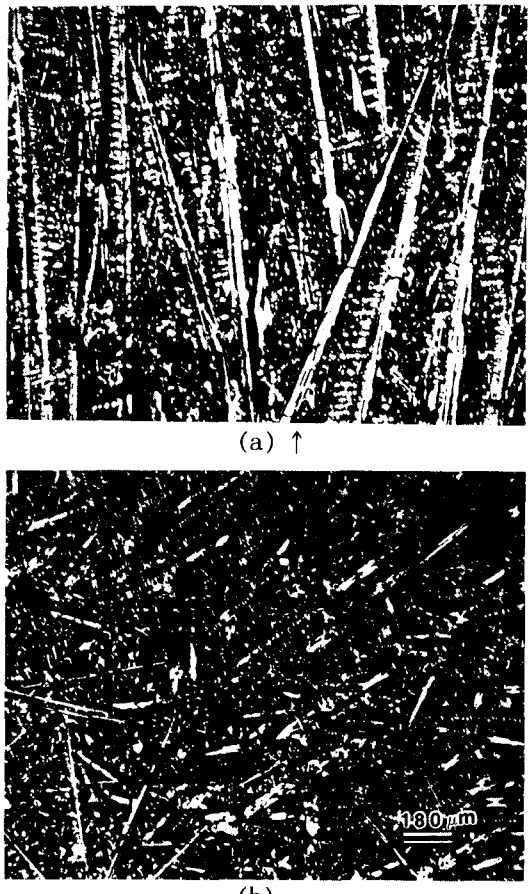

(a) ↑

(b)

Fig. 4. Microstructures of the unannealed $YBa_2Cu_7O_X$ ingot at low magnification (50×); (a) longitudinal section (↑ : growth direction) and (b) transverse section.

Fig. 5. Microstructure of the annealed $YBa_2Cu_7O_X$ sample (200×) ; (G) $YBa_2Cu_3O_X$ and Y_2BaCuO_5, (W) CuO.

path will stop at p1. If equilibrium is not achieved, there would be excessive BaO and CuO oxides in the liquid, due to the incomplete reaction of the 211 phase. As a result, the end point would shift toward e1, producing the $BaCuO_2$ and CuO eutectic structure observed in the matrix, as shown in Fig. 6 (b).

3.3. *$YBa_5Cu_{11}O_X$ composition*

An ingot 4 cm in length was produced, and was composed of two distinctive areas. In the bottom area (two third of the total ingot length), long and thin 211 crystals grew in the matrix. The equiaxed 011 dendrites were scattered in the matrix, in which the $BaCuO_2$-CuO eutectic structure was developed (see Fig. 7 (b)). According to EDX data from this area, most of needle-shaped crystals were 211. However, the needle-shaped crystals of the YBCO phase, without the 211 phase, were formed in the top area of the ingot and matrix appeared to be a single phase (011), without the CuO or eutectic structure (bottom half of Fig. 7(a)).

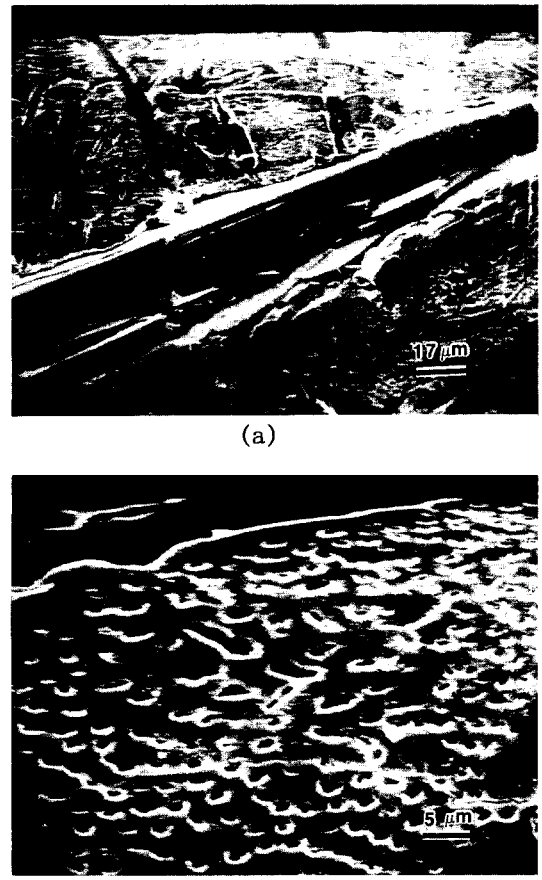

Fig. 6. SEM images of the unannealed $YBa_2Cu_7O_X$ sample ; (a) the needle-shaped $YBa_2Cu_3O_X$ grain and (b) CuO (discontinuous phase)-$BaCuO_2$ eutectic structure.

(a) ↑

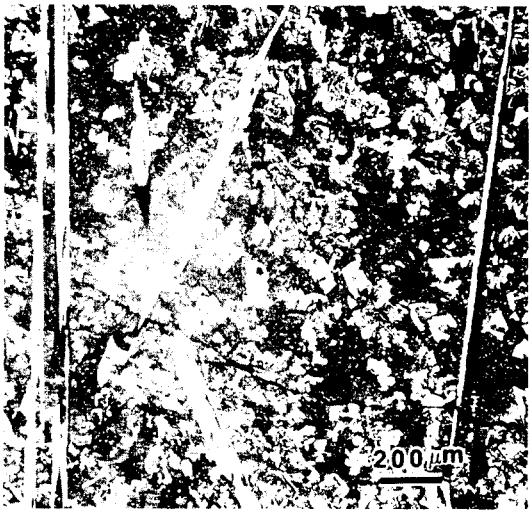

(b) ↑

Fig. 7. Microstructures of the unannealed longitudinal section of the $YBa_5Cu_{11}O_X$ ingot (50×) ; (a) the top area of the ingot and (b) the bottom area of the ingot (↑ : growth direction).

The XRD data confirmed these EDX results. The peak intensities of the YBCO and 011 phases increased in the top area, with no peak of the 211 phase.

If the liquid is cooled under euqilibrium conditions, the YBCO primary phase should form without the 211 phase, and the 011 phase should form with the YBCO phase on the boundary curve. Then the 001 phase, with the YBCO and 011 phase, will precipitate at e1. The resultant ingot, however, showed a quite different microstructure. The unexpected 211 phase in the ingot indicates that either the primary phase region is incorrect or that liquid temperature fluctuations caused the 211 phase to precipitate. (The fine control of the temperature was very difficult in these experiments). The precipitated YBCO phase may resolve to the 211 phase when the liquid temperature increases. The 211 phase precipitation would produce a BaO-CuO rich liquid. If the liquid temperature decreased, the YBCO and 011 phases would precipitate along the YBCO-011 phase boundary as an eutectic-like structure (bottom half of Fig. 7(a)) and consequently the CuO-$BaCuO_2$ eutectic structure would be formed (at e1) due to low growth rate, as shown in top half area of Fig. 7 (a). This YBCO grain was faceted and directly formed from the liquid, not by the peritectic reaction. Therefore it is expected that the faceted YBCO grain in this ingot was formed by the solute diffusion through the liquid [15,16]. The band microstructure shown in Fig. 7 (a) might be caused by a poor liquid temperature control or an unsteady vertical movement mechanism.

4. Conclusions

1. No faceted grains, which grew along the solidification direction, including the YBCO phase were observed for the $YBa_2Cu_3O_X$ composition. Typical microstructures consisted of Y_2BaCuO_5 grains in the envelopes of the YBCO phase which was formed by the peritectic transformation.

2. The directional alignment of the needle phases was most prominent for the $YBa_2Cu_7O_X$ composition. The Y_2BaCuO_5 and $YBa_2Cu_3O_X$ phases often grew as long, needle-shaped crystals in the matrix of $CuO-BaCuO_2$ eutectic structure.

3. Two distinctive areas formed in the $YBa_5Cu_{11}O_X$ ingot. The bottom of this ingot contained of needel-shaped Y_2BaCuO_5 grains and $BaCuO_2$ dendrites. The top portion formed needle-shaped $YBa_2Cu_7O_X$ grains in the matrix of the $BaCuO_2$ single phase, with no Y_2BaCuO_5 grains observed.

References

[1] J.G. Bednorz and K.A. Muller , Z. Phys. B : Condens. Matter 64 (1986) 189.

[2] M.K. Wu, J.R. Ashburn, C.J. Torng, P.H. Hor, R.L. Meng, L. Gao, Z.J. Huang, Y.Q. Wang and C.W. Chu, Phys. Rev. Lett. 58 (1987) 908.

[3] J.W. Ekin, Adv. Ceram. Mater. 2 (1987) 586.

[4] H. Mazaki, M. Takano, Y. Ikeda, Y. Bando, R. Kanno, Y. Takeda and O. Yamamoto, Jpn. J. Appl. Phys. 26 (1987) L1749.

[5] T. H. Geballe and J.K Hulm, Science 239 (1988) 22.

[6] K. Murata, K. Hayashi, Y. Honda, M. Tokumoto, H. Ihara and M. Hirabayashi, Jpn. J. Appl. Phys. 26 (1987) L1941.

[7] H.M. Jang, K.W. Moon and S. Baik, Jpn. J. Appl. Phys. 28 (1989) L1223.

[8] S. Jim, T.H. Tiefel, R.C. Sherwood, M.E. Davis, R.B. VanDovor, G.W. Kammlott, R.A. Fastnacht and H.D. Keith, Appl. Phys. Lett. 52 (1988) 2074.

[9] J.E. Blendell *et al.*, Adv. Ceram. Mater. 2 (1987) 512.

[10] W. Wong-Ng *et al.*, Adv. Ceram. Mater. 2 (1987) 624.

[11] M.J. Shapiro, K.L. More, W.J. Lackey, J. A. Hanigofsky, D.N. Hill, W.B. Carter, E. K. Barefield, E.A. Judson, D.F. O'Brien, R. Patrick, Y.S. Chung and T.S. Moss, J. Am. Ceram. Soc. 74 (1991) 2021.

[12] C.T. Cheung and E. Ruckenstein, J. Mater. Res. 4 (1989) 1.

[13] T. Hashimoto, K. Fueki, A. Kishi, T. Azumi and H. Koinuma, Jpn. J. Appl. Phys. 27 (1988) L214.

[14] T. Aselage and K. Keefer, J. Mater. Res. 3 (1988) 1279.

[15] D.H. St. John and L.M. Hogan, Acta Metallurgica 25 (1977) 77.

[16] T. Izumi, Y. Nakamura and Y. Shiohara, J. Mater. Res. 7 (1992) 1621.